

## THERMODYNAMIC ANALYSIS OF A KALINA POWER UNIT DRIVEN BY LOW TEMPERATURE HEAT SOURCES

by

**Periklis A. LOLOS and Emanuil D. ROGDAKIS**

Original scientific paper  
UDC: 662.997:66.045.5  
DOI: 10.2298/TSCI0904021L

*In this paper the operation of a reversible Kalina power cycle driven by low temperature heat sources has been studied. A numerical model has been developed to analyze thermodynamically the proposed cycle and to represent it in temperature-entropy and temperature-enthalpy diagrams. A parametric study has been conducted in order to specify the optimum values of the main parameters, i. e. low pressure, condensation and heat source temperature with respect to thermal performance. An improved configuration using a counter-current absorber instead of the conventional condenser (co-current absorber) has been proposed which has significantly higher efficiency and work output. Finally, simple equations have been derived which link the main parameters of the unit with the theoretical thermal efficiency.*

Key words: *Kalina cycle, thermodynamic analysis, ammonia-water*

### Introduction

The Kalina cycle is similar to the Rankine cycle except that it heats two fluids, such as ammonia and water, instead of one. In contrary to one-fluid working media such as water or pentan, the ammonia-water mixture boils over a large temperature range by predefined pressure. Single one phase media boils and condense over constant temperature. In the Kalina cycle the mixture boils over a constantly raising temperature and condenses over a constantly diminishing temperature: the ammonia in the mixture begins to vapor first and as it boils off, its concentration decreases, and the boiling temperature of the mixture increases. This reduces the temperature mismatch between the heat source and the fluid in the boiler and allows an efficiency rise in the cycle comparing to a single fluid medium. The mixture's composition varies throughout the cycle so that each time the best possible matching between the working medium and the heat source can be achieved.

The first publication on a Kalina cycle included a combined cycle application using waste heat to produce power [1]. It uses  $\text{NH}_3\text{-H}_2\text{O}$  as a working medium and shows a thermodynamic efficiency considerably higher than that of a Rankine cycle.

Rodgakis [2] and Rodgakis *et al.* [3] described and parametrically analyzed a Kalina power cycle driven by a heat source of high to moderate temperatures which works with three pressure levels. In this cycle the heat contained in the exhaust steam is used to drive a "thermal compressor" allowing a higher turbine expansion ratio and a higher efficiency.

Kalina *et al.* [4] presented a power cycle for geothermal applications. In this study, it was shown that the Kalina cycle has a higher power output for a specified geothermal heat source compared with organic Rankine cycles and steam flash cycles.

In the present study, the operation of a reversible dual pressure Kalina power cycle driven by low temperature heat sources, similar to the one installed in Husavic, Iceland [5], has been thermodynamically analyzed. The complete process has been represented in detail in temperature-entropy and temperature-enthalpy diagrams. An improved configuration has been proposed which appears to have a better performance. Finally, a parametric analysis of the cycle is conducted and correlations have been developed which link the operational parameters with the theoretically achieved efficiency.

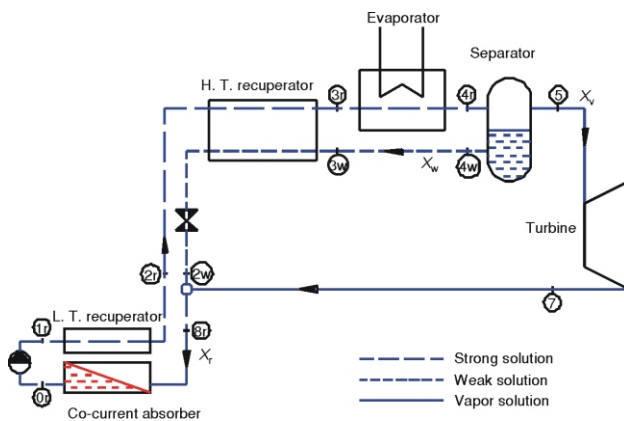


**Figure 1. Schematic arrangement of a Kalina power cycle with a co-current absorber – Configuration 1**

Starting at the outlet of the absorber (state 0) the strong solution of a mass fraction  $X_r$  is saturated at a low pressure  $p_L$ . This stream is pumped to a high pressure by the feed pump (state 1r). The feed stream is preheated in the low temperature (state 2r) and the high temperature (state 3r) recuperators before entering the evaporator. In the evaporator the mixture is heated to  $T_H$ , where it is partially vaporized (state 4r). This mixed-phase fluid is sent to the separator where the basic solution is separated into an enriched vapor  $X_v$  (state 5) and a weak liquid solution  $X_w$  (state 4w). The high-pressure, strong saturated vapor from the separator drives the turbine as the vapor rapidly expands and cools to a low temperature, low pressure exhaust (state 7). The saturated liquid solution (state 4w), after recuperating some of the heat at the high temperature recuperator, is throttled down to a low pressure (state 2w). Then the expanded stream (state 7) mix with the weak stream (state 2w), condenses and

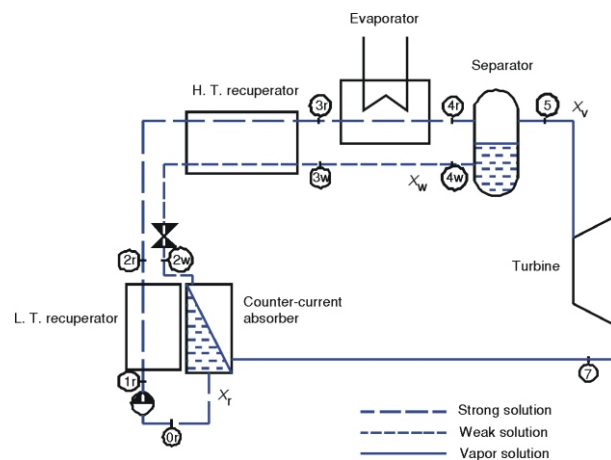


**Figure 2. Schematic arrangement of a Kalina power cycle with a co-current absorber – Configuration 2**

### Description of the cycle

A power generation unit based on a Kalina cycle includes the main parts: low- and a high temperature co-current heat exchangers (recuperators: H. T. – high temperature; L. T. – low temperature), evaporator, separator, turbine, and condenser (fig. 1).

This arrangement is based on a Kalina power unit installed in Husavic, Iceland. A brief description of the cycle follows (fig. 1)

Starting at the outlet of the absorber (state 0) the strong solution of a mass fraction  $X_r$  is saturated at a low pressure  $p_L$ . This stream is pumped to a high pressure by the feed pump (state 1r). The feed stream is preheated in the low temperature (state 2r) and the high temperature (state 3r) recuperators before entering the evaporator. In the evaporator the mixture is heated to  $T_H$ , where it is partially vaporized (state 4r). This mixed-phase fluid is sent to the separator where the basic solution is separated into an enriched vapor  $X_v$  (state 5) and a weak liquid solution  $X_w$  (state 4w). The high-pressure, strong saturated vapor from the separator drives the turbine as the vapor rapidly expands and cools to a low temperature, low pressure exhaust (state 7). The saturated liquid solution (state 4w), after recuperating some of the heat at the high temperature recuperator, is throttled down to a low pressure (state 2w). Then the expanded stream (state 7) mix with the weak stream (state 2w), condenses and

form the basic solution completing the cycle; this can be achieved either through a co-current absorber (fig. 1) or through a co-current absorber (fig. 2). The characteristics of each one of these arrangements are described thoroughly in the next chapters.

## Cycle modelling

### Configurations and general assumptions

Two cycle configurations have been studied in this paper. The model used for the basic cycle configuration is shown in fig. 1. Three independent variables are sufficient to determine the operation of the cycle. The independent variables are:

- cycle low pressure,  $p_L$ ,
- cycle minimum temperature  $T_L$  (temperature at condenser exit), and
- cycle maximum temperature  $T_H$  (temperature at boiler exit).

Following streams are involved in the cycle:

- a weak solution of mass  $m_w = g$  kg and mass fraction  $X_w$  (change 2w-4w),
- a strong solution of mass  $m_r = (1 + g)$  kg and mass fraction  $X_r$  (change 1r-4r), and
- a rich vapor stream of mass  $m_v = 1$  kg and mass fraction  $X_r$  (change 5-7).

Following assumptions were used in the cycle modeling:

- all processes taking place in the power cycle, apart from pumps, throttling valves and the turbine, are considered as constant pressure changes,
- the strong mixture at condenser exit (state 0) and prior to enter the evaporator (state 3r) are at saturated condition,
- the weak mixture after its throttling to the low pressure (state 2w) is at saturated condition, and
- heat losses in the piping and the heat exchangers are neglected.

Using the variables and assumption listed, the properties of all state points in the cycle can be determined.

For a binary mixture according to the Gibbs law, two intensive properties and the composition of the mixture are sufficient to establish all the other properties. In case of a two-phase region (saturated condition) two intensive properties (pressure and temperature) or an intensive property and the composition of the mixture are sufficient.

The thermodynamic properties of the mixture  $\text{NH}_3\text{-H}_2\text{O}$  are calculated using the equations of Ziegler and Trepp [6] which are valid for pressures up to 50 bar.

### State point calculation

A computer code has been developed in order to calculate the thermodynamic properties of each state point of the cycle.

The strong solution is partially vaporized in the boiler. A mass balance gives the vapor mass fraction ( $vmf$ ) of point 4r:

$$vmf_{4r} = \frac{X_r \cdot x_{\text{satliq}}(T_{4r}, p_{4r})}{x_{\text{satvap}}(T_{4r}, p_{4r}) - x_{\text{satliq}}(T_{4r}, p_{4r})} \quad (1)$$

The enthalpy of point 4r (per mass unit of the rich solution) is calculated by the following relation:

$$h_{4r} = (1 - vmf_{4r})h_{\text{satliq}}(T_4, p_4) + vmf_{4r}h_{\text{satvap}}(T_4, p_4) \quad (2)$$

$x_{\text{satvap}}(T, p)$  and  $x_{\text{satliq}}(T, p)$  are functions in the program to calculate the concentration of ammonia in the vapor and liquid mixture, respectively, given the pressure and the temperature.

The weak liquid stream from the H. T. recuperator (point 2w) and the vapor stream expanded in the turbine (point 7) mix to form the strong solution at state 8r (configuration with a co-current absorber). The mixing is assumed to be a constant total enthalpy process.

A simple energy balance allows the determination of enthalpy at state 8r (per mass unit of the rich solution):

$$m_r h_{8r} = m_w h_{2w} + m_v h_7$$

$$h_{8r} = \frac{g h_{2w} + 1 h_7}{1 + g} \quad (3)$$

### Basic equations

The enthalpy and entropy as well as heat quantities involved in every point of the process are reduced for 1 kg of vapour expanded in the turbine. The analysis technique, initially developed for a high temperature triple pressure Kalina cycle [7], is based on an assumption that in every point of the process two streams of different  $\text{NH}_3$  concentration flow in a co- or counter-current arrangement and exchange heat between them and the surrounding. Further, in every cross-section of the flow the two phases are considered to be at saturated condition and in thermodynamic equilibrium.

#### Mass balance

Mass quantity of  $(1 + g)$  kg strong solution flows in the evaporator and will be separated to 1 kg vapor mixture and  $g$  kg of weak solution. A mass balance of the volatile component in the separator gives the mass quantity of the weak solution  $g$ :

$$g \frac{1X_v - X_r}{X_r - X_w} = \frac{gX_w - (1 + g)X_r}{X_r - X_w} \quad (4)$$

1 kg  $\text{NH}_3$  vapor

#### Boiler heat transfer

$$q_{in} = h_5 - h_2 \quad (5)$$

#### Absorber heat rejection

$$q_{abs} = h_7 - h_2 \quad (6)$$

#### Work output

$$w_t = h_5 - h_7 \quad (7)$$

#### Thermal efficiency

$$\eta = \frac{w_t}{q_{in}} \quad (8)$$

All heat quantities calculated are based on 1 kg of vapor expanded in the turbine.

## Results and discussion

### Representation in $T$ - $s$ and $T$ - $h$ diagrams

The cycle has been graphically represented in temperature-entropy ( $T$ - $s$ ) and temperature-enthalpy ( $T$ - $h$ ) diagrams. Using these diagrams the temperature level of each thermodynamic

process can be directly depicted in the abscise allowing thus a direct conclusion about the feasibility of heat exchange between the processes. Further, in the  $T-h$  diagram the heat amount as well as the work involved in each process is represented as simple length in the enthalpy axis whereas in the  $T-s$  diagram heat or work is represented as an area.

In the  $T-h$  and  $T-s$  diagrams the equilibrium curves for the saturated liquid and vapor states of the pure components (ammonia and water) are drawn for both pressure levels.

For the construction of the equilibrium curves for each pressure level following procedure is applied: the saturation temperatures for the pure components are calculated. Using a temperature step between these temperatures, enthalpy, entropy and mass fractions of the two saturated phases in equilibrium are determined.

In figs. 3 and 4 the  $T-s$  and  $T-h$  diagrams of the power cycle (configuration with the co-current absorber) are displayed. The combination of the curves 2r-3r-4r (strong solution) and 2w-3w-4w gives a resultant curve 2-3-5 that can be found as follows.

For every temperature take the entropy (or enthalpy) difference between the corresponding strong and weak solutions and multiply this value by  $g$ . Add the value of this product to the entropy (or enthalpy) of the strong solution and thus define the entropy (or enthalpy) of an auxiliary stream, of mass flow rate 1 [kg], that requires the same heat quantities as the combination of the two real streams of the strong and weak solutions.

The required heat amount for every part of the power cycle can be depicted from the diagrams under following conditions:

- the thermodynamic limit between the evaporator and the H. T. recuperator is the boiling temperature of the strong solution (state 3),
- the stream of the weak solution after the separator which is warmer than the temperature of state 3 is considered as part of the evaporator,
- the weak stream after its expansion (state 2w) is at saturated condition; this temperature is also the thermodynamic limit between the H. T. recuperator and the condenser (the influence of the throttling valve is negligible), and
- the stream of the strong solution which is colder than the temperature of point 2w is considered as part of the condenser.

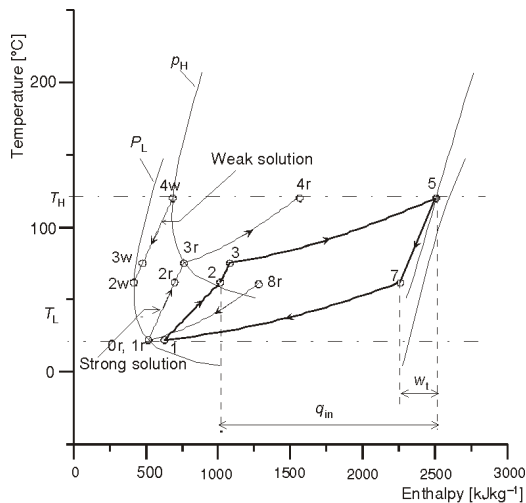


Figure 3.  $T-h$  diagram of the power cycle with a co-current absorber (Configuration 1)

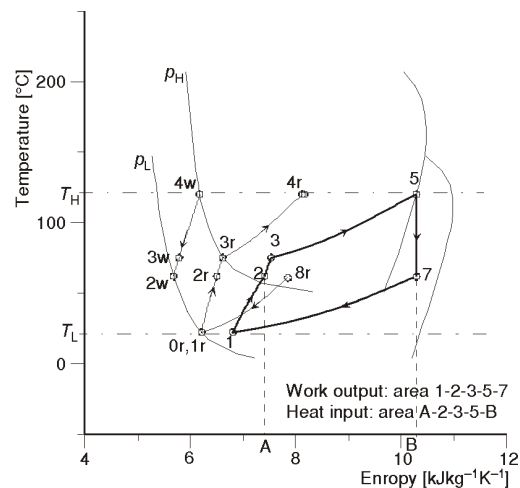


Figure 4.  $T-s$  diagram of the power cycle with a co-current absorber (Configuration 1)

### Configuration with a co-current absorber

Figures 3 and 4 show the  $T$ - $s$  and  $T$ - $h$  diagrams of the configuration with a co-current absorber. The line 4w-2w describes the change of the weak stream coming from the separator. The temperature of state 2w dictates the temperature at the exit of the turbine. The line 1r-4r describes the change of the strong solution coming from the absorber. Line 8r-1r describes the equivalent flow (reduced to 1 kg of strong solution) of the absorption of 1 kg of vapor from  $g$  kg of weak solution. The entire power cycle reduced to 1 kg of the vapor expanded in the turbine is described by the line 1-2-3-5-7-1.

Using the  $T$ - $s$  diagram the heat exchange feasibility between the processes can be succeeded by a simple comparison of the slopes of the heat accepting (curve 1r-2r-3r-4r) and the heat donating lines (curves 4w-3w-2w and 8r-1r). In this way with reference to fig. 3 the heat needed to drive the unit is evaluated as follows.

For temperature levels below the lowest temperature of the weak solution ( $T_2$ ) the heat quantity required for the operation of the L. T. heat exchanger is given by the co-current absorber. So an external heat source up to  $T_2$  is not required. For temperature levels above  $T_2$  the required heat to drive the H. T. recuperator and the evaporator is given by an external heat source.

### Configuration with a co-current absorber

Figures 5 and 6 show the temperature-enthalpy and temperature-entropy diagram of the configuration with a co-current absorber. Line 2w-1w describes the equivalent flow of the absorption process, while line 7-2 describes the resulting stream of 1 kg of vapor expanding in the turbine within the temperature area of the absorber. All other changes shown are identical to the cycle with a co-current absorber.

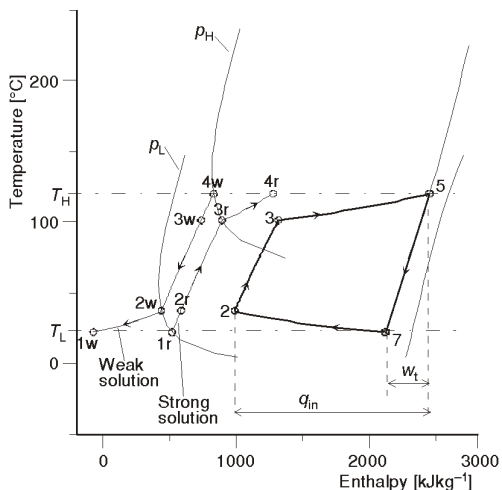


Figure 5.  $T$ - $h$  diagram of the power cycle with a co-current absorber (Configuration 2)

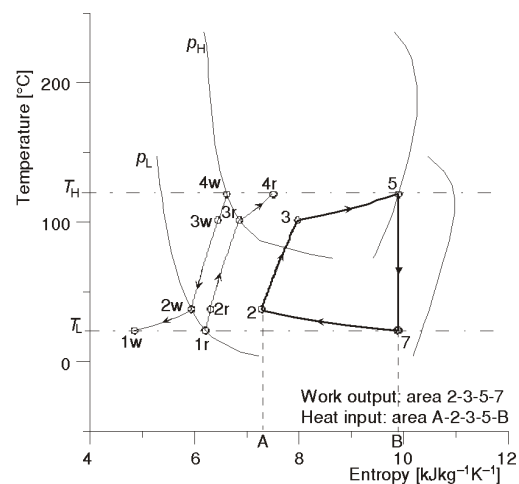


Figure 6.  $T$ - $s$  diagram of the power cycle with a co-current absorber (Configuration 2)

### Case studies examined

Both power cycle configurations were evaluated for following parameters:

**Table 1. Power cycle specifications and performance**

Cycle parameter	Configuration 1 (co-current absorber)	Configuration 2 (co-current absorber)
High pressure [bar]	21	36
Strong solution mass fraction $X_r$ [%]	64	64
Weak solution mass fraction $X_w$ [%]	38	52
Vapor mass fraction $X_v$ [%]	93	96
Mass ratio (kg strong solution per kg vapor expanded in the turbine)	1.9	2.7
Net heat input $q_{in}$ (kJ/kg vapor)	1496.8	1468.7
Net heat rejection $q_{abs}$ (kJ/kg vapor)	1246.9	1139.2
Work produced $w_T$ (kJ/kg vapor)	249.9	329.5
Efficiency $\eta$ [%]	16.7	22.4
Carnot efficiency [%]	25	

- low pressure,  $p_L = 5$  bar,
- minimum temperature  $T_L = 22$  °C , and
- maximum temperature  $T_H = 120$  °C.

The required heat quantity for the operation of the power cycle, produced work, and theoretical efficiency for the cases/configurations already described are listed in tab. 1.

The configuration with the co-current absorber, for the initial parameters listed above, has a ca. 25% higher efficiency and ca. 30% higher power output than the configuration with the co-current absorber.

The cycle efficiency and the produced work per kg vapor for various values of the low pressure are plotted in figs. 7 and 8 for the two configurations. For given maximum and minimum temperature of the cycle raising the low pressure causes a reduction of the produced work and the efficiency of the unit. Configuration with a co-current absorber is more sensible to

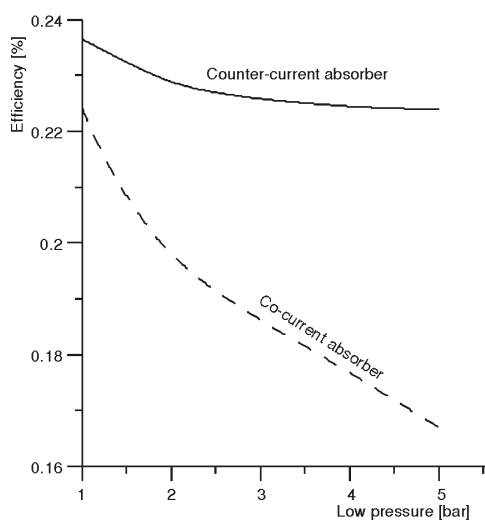


**Figure 7. Effect of the low pressure on the cycle efficiency**

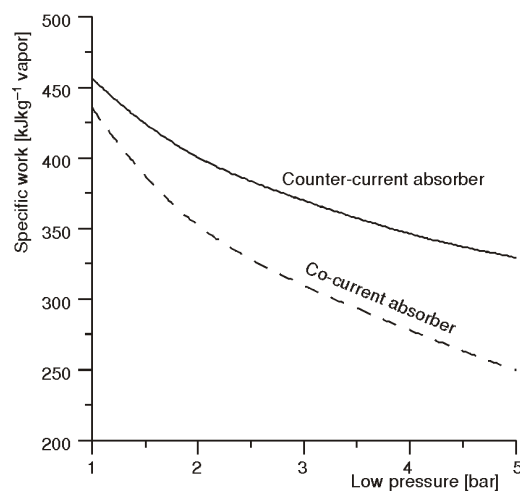


**Figure 8. Effect of the low pressure on the work output**

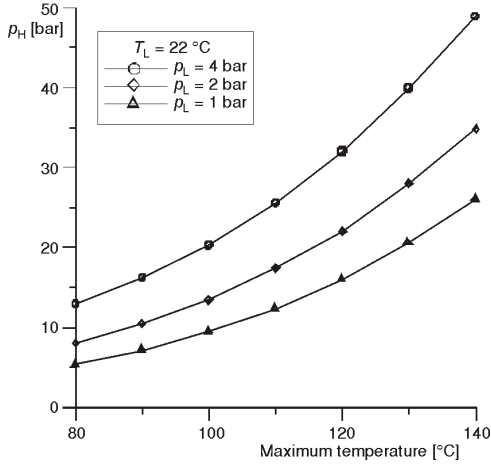


**Figure 9. High pressure vs. maximum temperature of the cycle for fixed values of the low pressure and the minimum temperature**

changes of the low pressure regarding efficiency and produced work than the configuration with a co-current absorber.

Under the operating parameters listed above the highest values for the cycle efficiency and work output have been achieved at  $p_L = 1$  bar and are  $\eta = 22\%$ ,  $w_T = 435$  kJ/kg for the configuration 1 and  $\eta = 23.6\%$ ,  $w_T = 456$  kJ/kg for the configuration 2.

Configuration 2 (with a co-current absorber) was thoroughly examined.

Figure 9 shows the relationship between the high pressure  $p_H$  and the maximum temperature  $T_H$  of the unit for three values of the low pressure and for given minimum temperature  $T_L$ . The high pressure has been correlated in terms of the three independent variables of the unit,  $T_H$ ,  $T_L$ , and  $p_L$  according to:

$$p_H = a_1 b_1 T_H c_1 T_H^2 \quad (9)$$

$$a_1 = \frac{16.47}{1.366} \frac{4.33 p_L}{10^2 T_L} \quad (10)$$

$$b_1 = (0.42 + 0.08 p_L)(1.3604 - 1.644 \cdot 10^{-2} T_L) \quad (11)$$

$$c_1 = (0.42 \cdot 10^{-3} + 7.38 \cdot 10^{-4} p_L)(1.3234 - 1.474 \cdot 10^{-2} T_L) \quad (12)$$

Figure 10 shows the influence of the minimum temperature  $T_L$  on the efficiency of the unit for fixed values of the other parameters. Cycle efficiency rises as minimum temperature decreases which is due to a lower heat amount required to drive the unit.

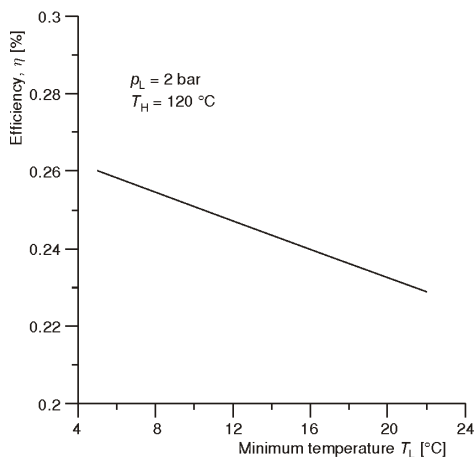


**Figure 10. Theoretical cycle efficiency vs. minimum temperature of the cycle for fixed values of the low pressure  $p_L$  and the maximum temperature of the cycle  $T_H$**

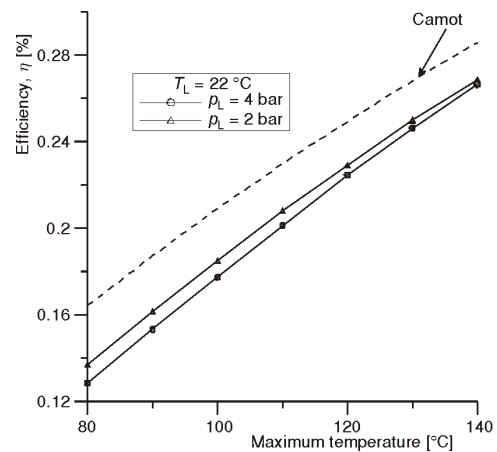


**Figure 11. Theoretical cycle efficiency vs. maximum temperature of the cycle for fixed values of the low pressure  $p_L$  and the minimum temperature  $T_L$**

Figure 11 shows how the theoretical efficiency of the cycle changes with the maximum temperature  $T_H$  for fixed values of the other parameters, for two values of the low pressure  $p_L$ . It can be seen that the ratio  $\eta/\eta_c$  (cycle efficiency to Carnot efficiency) increases as  $T_H$  increases.

The efficiency  $\eta$  has been calculated for a great number of combinations of the minimum temperature  $T_L$  (12 to 22 °C) and low pressure  $p_L$  (1 to 4 bar) and following correlations have been derived linking the efficiency with independent variables of the cycle:

$$\eta = a_2 + b_2 T_H + c_2 T_H^2 \tag{13}$$

$$a_2 = -0.049 - 0.0022 T_L \tag{14}$$

$$b_2 = 0.0035 - 0.92^{1/p_L} \tag{15}$$

$$c_2 = -2.36 \cdot 10^{-6} - 2.19 \cdot 10^{-6} p_L + 3.14 \cdot 10^{-7} p_L^2 \tag{16}$$

The variation of the produced work and the strong solution mass ratio (kg strong solution per 1 kg vapor) with the maximum temperature of the cycle, for three values of the low pressure and a fixed minimum temperature  $T_L = 22$  °C, are plotted in fig. 12.

Finally, fig. 13 shows the difference between strong and weak solution given the low pressure and minimum temperature over a range of maximum temperatures. The change is plotted over a variety of low pressures  $p_L = 1, 2, 4,$  and  $5$  bar which corresponds to a strong solution of mass fraction  $X_r = 34, 45, 59,$  and  $65\%$ , respectively.

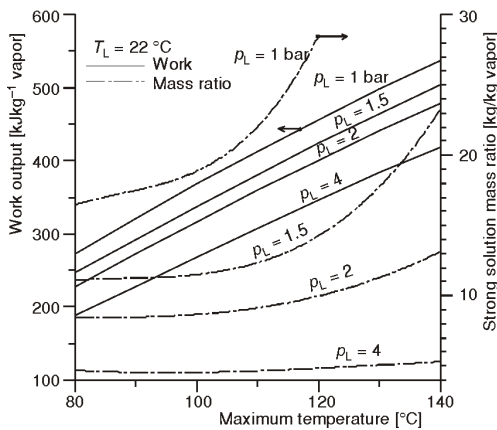


Figure 12. Variation of (a) the produced work and (b) the ratio of the strong solution mass per kg vapor, in terms of the maximum temperature for fixed values of the minimum temperature and low pressure of the cycle

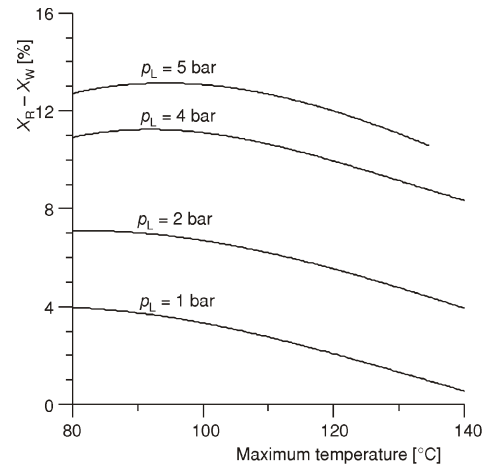


Figure 13. Difference of the strong to the weak solution  $X_r - X_w$  in terms of the maximum temperature of the cycle ( $T_H$ ) for fixed minimum temperature  $T_L = 22$  °C

### Conclusions

In the present paper, the operation of a reversible Kalina power cycle driven by low temperature heat sources has been studied. The cycle configuration is based on a Kalina power unit installed in Husavic, Iceland.

An analytical model has been developed and used to thermodynamically analyze the low heat source Kalina cycle. The medium used to recover rejected heat was  $\text{NH}_3\text{-H}_2\text{O}$ . Each process of the cycle, which involve a two stream flow has been thermo-dynamically analyzed with respect to flow arrangement and expressed through an equivalent single flow stream.

The variations of the thermodynamic state of the binary mixture  $\text{NH}_3\text{-H}_2\text{O}$  have been graphically represented in  $T$ - $h$  and  $T$ - $s$  diagrams. All heat quantities have been reduced to 1 kg vapor expanded in the turbine. Graphical representation of heat recovery cycles in  $T$ - $s$  and  $T$ - $h$  diagrams enable quick and reliable estimation of thermal power and heat exchanged between mixture and the environment. This gives the opportunity to scientists and engineers to dimensioning such installations and making further improvements.

An improved configuration using a counter-current absorber instead of the conventional condenser (co-current absorber) has been proposed which has significantly higher efficiency and work output. According to the parametric analysis conducted, the efficiency of the cycle depends on following parameters: the ratio of the heat source to heat sink temperatures  $T_{\text{max}}/T_{\text{min}}$ , the low pressure of the process  $p_L$  as well as the type of absorber-condenser. As revealed, for fixed minimum and maximum temperatures, cycle efficiency can be maximized for a counter-flow absorber and for an expansion pressure of  $p_L = 1$  bar.

Simple equations have been derived, which link the theoretical efficiency with the main parameters of the unit.

## Nomenclature

$\eta$	– efficiency, [%]
$h$	– specific enthalpy [ $\text{kJkg}^{-1}$ ]
$m$	– mass, [kg]
$p$	– pressure, [bar]
$q$	– specific heat, [ $\text{kJkg}^{-1}$ ]
$s$	– specific entropy [ $\text{kJkg}^{-1}\text{K}^{-1}$ ]
$T$	– temperature [ $^{\circ}\text{C}$ ]
$vmf$	– vapor mass fraction (kg vapor per kg mixture), [–]
$w$	– specific work [ $\text{kJkg}^{-1}$ ]
$X$	– mass fraction of the liquid mixture ( $\text{kgNH}_3$ per kg liquid mixture), [–]
$g$	– mass of the weak solution per 1 kg of the vapor

## Subscripts

H	– high pressure
L	– low pressure
r	– strong solution
w	– weak solution
v	– vapor
t	– turbine
in	– input
abs	– absorber
satvap	– saturated vapor
satliq	– saturated liquid

## References

- [1] Kalina, A. I., Combined Cycle and Waste Heat Recovery Power Systems Based on a Novel Thermodynamic Energy Cycle Utilizing Low-Temperature Heat for Power Generation, *Proceedings, Joint Power Generation Conference, Indianapolis, Ind., USA, 1983*, ASME Paper No. 83-JPGC-GT-3.
- [2] Rogdakis, E. D., Thermodynamic Analysis, Parametric Study and Optimum Operation of the Kalina Cycle, *International Journal of Energy Research*, 20 (1996), 4, pp. 359-370
- [3] Rogdakis, E. D., Antonopoulos, K. A., A High Efficiency  $\text{NH}_3\text{-H}_2\text{O}$  Absorption Power Cycle, *Heat Recovery Systems and CHP*, 11 (1991), 4, pp. 263-275
- [4] Kalina, A. I., Leibowitz, H. M., Application of the Kalina Cycle Technology to Geothermal Power Generation, *Geothermal Resources Council Transactions*, 13 (1989), pp. 605-611
- [5] Leibowitz, H. M., Mlcak, H. A., Design of a 2 MW Kalina Cycle Binary Module for Installation in Husavik, Iceland, *Proceedings, Geothermal Resources Council Annual Meeting, Reno, Nev., USA, 1999*, Vol. 23, pp. 75-80

- [6] Ziegler, B., Trepp, C., Equation of State for Ammonia-Water Mixtures, *International Journal of Refrigeration*, 7 (1984), 2, pp. 101-106
- [7] Kouremenos, D. A., Rogdakis, E. D., The Temperature – Entropy (or Enthalpy) and the Enthalpy-Entropy (Mollier) Diagrams of the Kalina Cycle., ASME Advanced Energy Systems Division, New York, USA, 1990, Vol. 19, pp. 13-19

Authors' affiliation:

**P. A. Lolos (corresponding author)**  
Laboratory of Applied Thermodynamics,  
Department of Thermal Engineering,  
School of Mechanical Engineering,  
National Technical University of Athens  
9, Heron Polytechniou Str., Zografou Campus  
15780 Athens, Greece  
E-mail: plolos@central.ntua.gr

*E. D. Rogdakis*  
Department of Thermal Engineering,  
School of Mechanical Engineering,  
National Technical University of Athens  
Athens, Greece